

Toolbox

***In vivo* Selective Cytoskeleton Dynamics Quantification in Interphase Cells Induced by Pulsed Ultraviolet Laser Nanosurgery**

**Julien Colombelli^{a,*}, Emmanuel G. Reynaud^a,
Jens Rietdorf, Rainer Pepperkok and Ernst
H.K. Stelzer**

*Cell Biology and Biophysics Unit, European Molecular
Biology Laboratory (EMBL), Meyerhofstrasse 1, D-69117
Heidelberg, Germany*

**Corresponding author: Julien Colombelli,
colombel@embl.de*

We report on the manipulation of intracellular filaments using a nanosurgery system based on a subnanosecond pulsed UV laser optimized for the localized severing of biological polymers. By inducing artificial catastrophe of selected microtubules (MTs), we perform shrinkage-rate measurements in interphase Ptk-2 cells throughout the entire cell. We quantify the impact of two labeling methods and three fluorescent markers, showing a 25% faster depolymerization with Alexa-488 tubulin compared with Rhodamine and yellow fluorescent protein (YFP) tubulins and a 20% higher variability induced by microinjection compared with stable transfection. Using EB3-GFP as a tip marker, we establish a new protocol to measure shrinkage rate, growth rate and rescue frequency simultaneously with high temporal and spatial specificity in live cells. As our analysis shows, laser-induced MT dynamics are physiologically relevant. The high statistical efficiency that the method offers in terms of numbers of measured events and therefore reduced standard deviations represents an important quantitative improvement in the measurement of dynamic instability parameters *in vivo*. We extend the application of the method by demonstrating induced dynamic behavior of actin-stress fibers after severing. This new method enables the quantitative investigation of cytoskeleton dynamics in a local confinement.

Key words: stress fibers, dynamic instability, microtubule, nanosurgery, pulsed laser

Received 19 May 2005, revised and accepted for publication 11 July 2005, published on-line 8 August 2005

The investigation of the biophysical properties of the cytoskeleton is a prerequisite to understanding a variety of biological processes and helps to validate predictions from models of dynamic cytoskeleton behavior. The organized behavior of the cytoskeleton in general and the microtubule (MT) network in particular are fundamental

^aThese authors contributed equally to this work.

biological activities (1) involved in the generation of cell shape, polarity, movement, morphogenesis, cell division and intracellular transport. Defects in cytoskeletal functions have been implicated in vascular diseases (2), neuronal degeneration (3,4) and cancer (5,6). The concept of dynamic instability (7) describes MTs as being in a permanent stochastic state of growth and shrinkage. This process seems to be vital, and therefore, polymerization dynamics of MTs (8) have been extensively investigated both *in vivo* and *in vitro*. Only a limited number of studies (9) successfully characterized the dynamic instability parameters in living cells. The main limitation has been the inability to resolve single MTs in fluorescence microscopy throughout the entire cell extent. The small number of MTs studied and the confinement of the field of view to the cell's border region have led to inconsistent and sparse data.

The need for *in vivo* methods results in an effort to push MT studies in a physiologically relevant cellular context. Various invasive techniques have been applied to perturb and study MTs, for instance, chemically with nocodazole or colchicines (10) to induce depolymerization in cells. Such techniques induce a dramatic perturbation of the cell shape and compromise the integrity and functionality of the cytoskeleton as well as the cell viability. In contrast, intracellular laser surgery proves to be a powerful tool when manipulating cellular content. Perturbation of MTs with ultraviolet (UV) rays has helped to characterize forces involved in spindle mechanisms and to show MTs behavior *in vivo* (11–16). Recent publications have reported great surgical accuracies *in vivo* using infrared or visible laser photodisruption to damage MT bundles (17–19), organelles (20), chromosomes (21) or neurons (22), but, as yet, no study has successfully applied pulsed UV lasers to quantify cytoskeleton dynamics.

We implemented a laser nanosurgery microscope (23), designed to sever biological materials *in vivo* with high precision. The mechanism of severing likely involves nonlinear absorption of highly focused laser pulses which results in confined ionization and ultimately forms plasma (discussed in 24).

In this study, we performed laser ablation of MTs in interphase Ptk-2 cells and characterized the severing of MTs induced by UV irradiation (UVI). We demonstrate variations in the dynamics of MTs as a consequence of three different labeling techniques. Using the MT GFP-EB3-tip marker (25),

we show that parameters of dynamic instability can be studied *in vivo* at specific time and space points without compromising the original cell shape and long-term viability. We exclude artifacts induced during the laser surgery by comparison with measurements in unperturbed cells using total internal reflection fluorescence (TIRF) microscopy and conclude that laser-induced catastrophe is physiological. We discuss our results in the light of the dynamic instability model and further demonstrate that the method can be efficiently applied to study other cytoskeletal components like actin. We propose this technique as a new method for the localized quantification of biological polymer dynamics *in vivo*.

Results

Intracellular laser nanosurgery of microtubules does not compromise cell viability

To investigate the effects of pulsed UVI on cell viability, we locally severed MTs in Ptk-2 cells stably transfected with a yellow fluorescent protein (YFP)- α -tubulin construct. Ultraviolet laser pulses induced artificial catastrophe of MTs and their subsequent shrinkage (Figure 1 and Supplementary Video 1 available as part of the online article from http://www.traffic.dk/suppmat/6_11.asp). We observe shrinkage only from the newly generated plus end towards the centrosome of the cell and can thereby determine the polarity of MTs. To estimate the consequences of such a perturbation of the MT cytoskeleton on the cell viability, we monitored the division fate of cells treated with UVI by time-lapse recordings over a period of 24 h. Thirty percent of the total number of cells present throughout the field of view underwent mitosis (6/20 cells) within 24 h of observation, while 50% (2/4 cells) of the UVI-treated cells divided within the same period (Figure S1 and Supplementary Video 2 available as part of the online article from http://www.traffic.dk/suppmat/6_11.asp).

Laser-induced MT-shrinkage rates depend on the labeling method

To assess the impact of three different tubulin-labeling methods on MT-shrinkage rates in mammalian interphase Ptk-2 cells *in vivo* (Figure 2), rhodamine tubulin and Alexa-488 tubulin were microinjected (26). We dissected MTs between 2 and 6 h after injection. Because of the high speed of line cutting (up to 1000 pulses per second, see Methods), MTs are considered to be dissected simultaneously in between two camera frames. The shrinkage rate of bulk MTs was analyzed by plotting the intensity changes along a line region of interest perpendicular to the cut, over time (Figure 1B). The rate of contrast change over time due to vanishing tubulin fluorescence is obtained by a linear manual fit of the contrast edge in the resulting kymograph image (Figure 1E), which is achieved with an accuracy of 5% on average. We measured average UVI-induced shrinkage velocities of $20.9 \pm 5.5 \mu\text{m}/\text{min}$ ($n = 136$) and $25.4 \pm 5.4 \mu\text{m}/\text{min}$ ($n = 131$) for rhodamine- and Alexa-488-labeled MTs, respectively (Figure 2A,B),

while in stably transfected YFP tubulin Ptk-2 cells (Figure 2C), the average shrinkage rate observed after UVI was $19.5 \pm 3.9 \mu\text{m}/\text{min}$ ($n = 106$). In a parallel set of experiments, we determined MT-shrinkage rates in unperturbed cells using TIRF microscopy on stably transfected YFP tubulin cells to be $22.5 \pm 10.2 \mu\text{m}/\text{min}$ ($n = 273$, Figure 4G). Laser-induced shrinkage was therefore measurable with high repeatability, and data collected over a large number of samples (373 MTs in 100 cells) show that the rates depend on the labeling method.

Laser-induced MT-shrinkage rates do not depend on the relative position of UVI in the cell

Ultraviolet irradiation was applied at different positions inside the cytoplasm of cells containing MTs labeled with different dyes (Figure 2D–F). The number of measurements at the relative site is plotted as a function of distance from the centrosome (Figure 2E). The histogram shows that results can be obtained for more than two-thirds of the distance that separates the cell edge from the centrosome, as reported in Figure 2(E). Measurements closer to the centrosome were not possible due to high background in this region in the widefield microscope. Microtubule shrinkage after laser-induced catastrophe was observable along the segments of MTs ranging from 2 to 10 μm (Figure 2F) and could be measured with high repeatability over a large number of samples ($n = 373$). We did not find any correlation between the subcellular position of the perturbation and the shrinkage rate (data not shown).

MTs rescue and regrowth after laser dissection

Transfected GFP-EB3 in Ptk-2 cells stably expressing tubulin YFP (Figure 3) allowed us to visualize the growing MT tips. Cells were visualized with a unique GFP filter set for a maximal recording speed. Cells were selected on the basis of the relative fluorescence level between the tips and the MT body to exclude cells that suffer from stabilization artifacts induced by overexpression. Only cells expressing fluorescence at higher levels at the tips than along the MT bodies and showing relatively short EB3 comets were processed in our experiments. After UVI, MT shrinkage occurred, and new tips appeared with time, highlighted by EB3-GFP (Figure 3B). Regrowth of MTs was observed throughout the entire region of irradiation (Figures 3C,D, see also Supplementary Video 3 available as part of the online article from http://www.traffic.dk/suppmat/6_11.asp). Regrowth could be instantaneous or delayed from the moment when the new tip appeared, as shown in Figure 3(E). We measured the growth rate of unmodified GFP-EB3 tips outside the area of irradiation (Figure 4D, inset) as well as regrowth rates of dissected MTs (Figure 4D). Preirradiated and postirradiated MT tips grow at similar speeds of $8.7 \pm 3.7 \mu\text{m}/\text{min}$ ($n = 72$) and $7.5 \pm 3.9 \mu\text{m}/\text{min}$ ($n = 88$), respectively, while the growth rate of unperturbed YFP-labeled MTs is $8.1 \pm 3.8 \mu\text{m}/\text{min}$ ($n = 240$, Figure 4H) as measured in TIRF experiments.

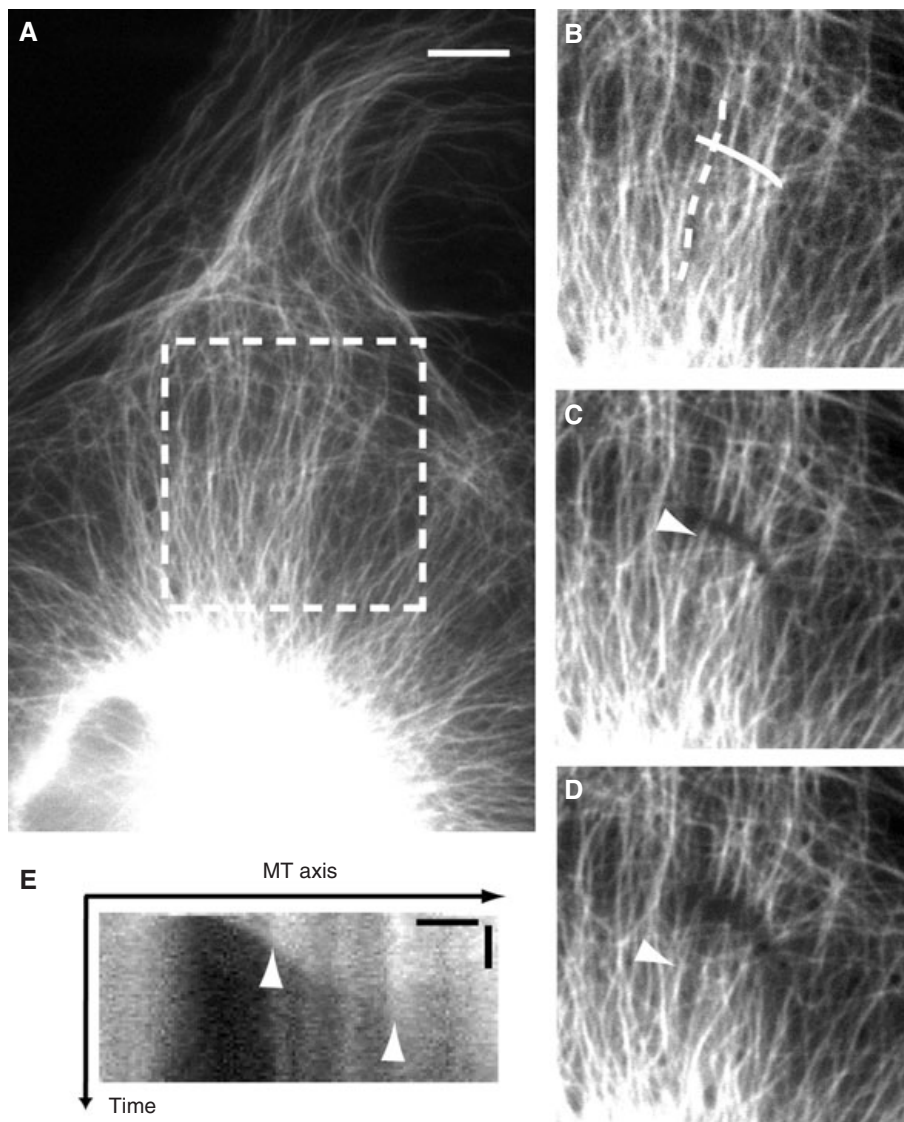


Figure 1: Ultraviolet laser irradiation induces microtubule catastrophe and depolymerization.

A) Fluorescent micrograph of a Ptk-2 cell stably transfected with yellow fluorescent protein (YFP)- α -tubulin recorded on an inverted epi-fluorescence microscope. The dashed square indicates the enlarged area shown in (B–D). B–D) Sequences of a microtubule shrinkage. The laser target path is indicated as a full white line in (B). C–D) show the same region 5.7 and 17 seconds after cutting. E) Kymograph obtained by plotting the intensity changes along the dashed line in (B) for each image of the sequence. The white arrowheads in (C–E) mark corresponding microtubule (MT) plus end positions in the kymograph and in the image sequence. The shrinkage process is linear with time, and its velocity can be measured with a simple linear slope fitted to the kymograph. Scale bars: 10 μ m in (A), 5 μ m horizontal and 5 seconds vertical in (E). See also Supplementary Video 1 available as part of the online article from http://www.traffic.dk/suppmat/6_11.asp.

Estimation of the rescue frequency after laser-induced catastrophe

Rescue of MTs after dissection was observed using GFP-EB3 as a marker localizing at new growing tips (see above). If T_R is the time elapsing from the UVI procedure until the appearance of a new tip, we define for each new tip the frequency of rescue as $F_R = 1/T_R$, which describes the rate at which MTs undergo rescue after laser-induced catastrophe. Figure 4(E) shows the distribution of values retrieved from 25 cells. F_R was measured to be 0.125 ± 0.083 events/second ($n = 357$ tips). The measurement was done manually by monitoring the number of frames separating UVI and each rescue event, with an uncertainty of \pm one frame (<0.5 seconds).

How to distinguish the severing of different cellular components

Because UV laser nanosurgery is not specific to MTs, we visually checked for the integrity of a variety of membranous

compartments *in vivo* after UVI using standard labeling procedures. The endoplasmic reticulum, Golgi apparatus and plasma membrane did not show any evident dynamic behavior after irradiation at the same experimental parameters used with MTs severing. The overall cell shape was unchanged for at least 5 min after UVI (data not shown). Mitochondria were apparently disrupted by UVI, as previously shown with different systems using femtosecond (20) or nanosecond (27) lasers. The actin cytoskeleton demonstrated an observable dynamic response. We transfected a green fluorescent protein (GFP)-actin construct into Ptk-2 cells, which allowed us to see the actin fibers or 'stress' fibers that assemble close to the lower plasma membrane. Performing UVI with the same experimental parameters as previously described for MTs, we demonstrated that severing stress fibers without damaging the plasma membrane can be efficiently achieved (Figure S2 and Supplementary Video 4 available as part of the online article from http://www.traffic.dk/suppmat/6_11.asp).

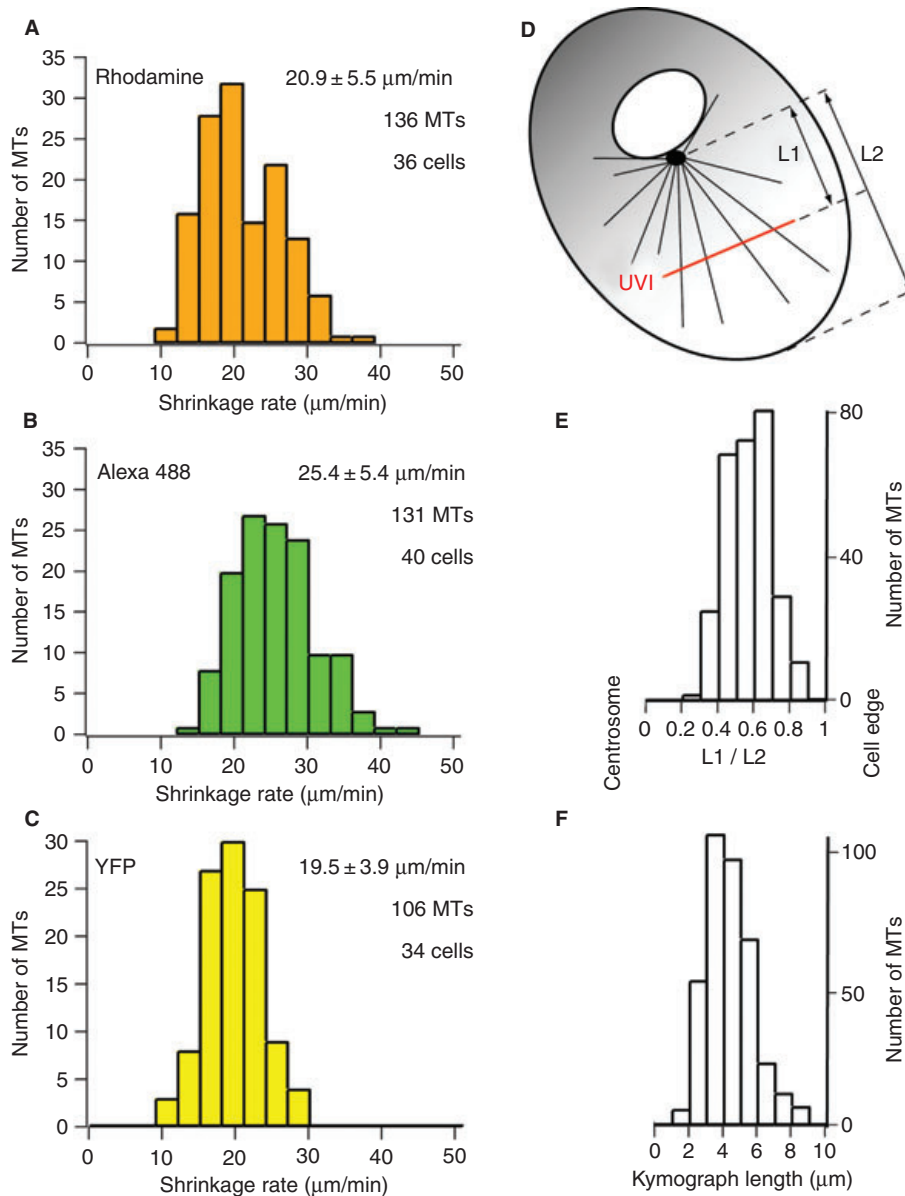


Figure 2: The *in vivo* rate of microtubule shrinkage depends on the labeling method. A–C) *In vivo* microtubule (MT) shrinkage rates for three different labeling methods: microinjection of rhodamine tubulin (A) or Alexa-488 tubulin (B) or with stably transfected yellow fluorescent protein (YFP) tubulin (C). In each histogram, the shrinkage rate is reported together with the total number of studied MT bundles and the number of cells used in the data evaluation. D) Cell schematic representing the relative position of the ultraviolet irradiation (UVI) target line in red. L1 is the distance from the centrosome to the UVI and L2 the distance from the centrosome to the cell edge. E) Histogram of the L1/L2 ratio for 373 shrinking MTs in 100 cells. F) Distribution of the length along which shrinkage was measurable for all the UVI procedures, i.e. the kymograph lengths, with an average of 4.1 μm.

Actin fibers were clearly dissected, as the UV-irradiated cell shows bundles of GFP-actin retracting from the spline cut and along the axis of the fibers. This phenomenon was also observed when performing MTs dynamics measurement. The non-linear retraction of actin fibers could influence the position of MTs, thereby preventing a good linear fit of MT shrinkage on kymographs. Cells showing simultaneous actin retraction and MT shrinkage were not considered for our MT dynamics study.

Discussion

Dynamic instability (7,8) has been extensively studied *in vitro* in the past decades. It defines MTs in a stochastic succession of growth and shrinkage phases with

transition states called rescue, from shrinkage to growth, and catastrophe, from growth to shrinkage. However, *in vivo* studies by time-resolved imaging, using either differential interference contrast (28) microscopy or fluorescently labeled polymers (29), have encountered severe practical limits. A major problem was the ability to resolve single fluorescent MTs, which was possible only at the thin cell edge (28,29). In consequence, because the spatial confinement of the events reduced the probability of performing a measurement, the number of evaluated events was not sufficient (Table 1), to derive relevant statistics and consistent values. One way to partially overcome these limits could be to use fluorescence speckle microscopy (30), and even though the evaluation of speckle data to obtain values for filament growth and shrinkage *in vivo* should be possible, such data has not been published until

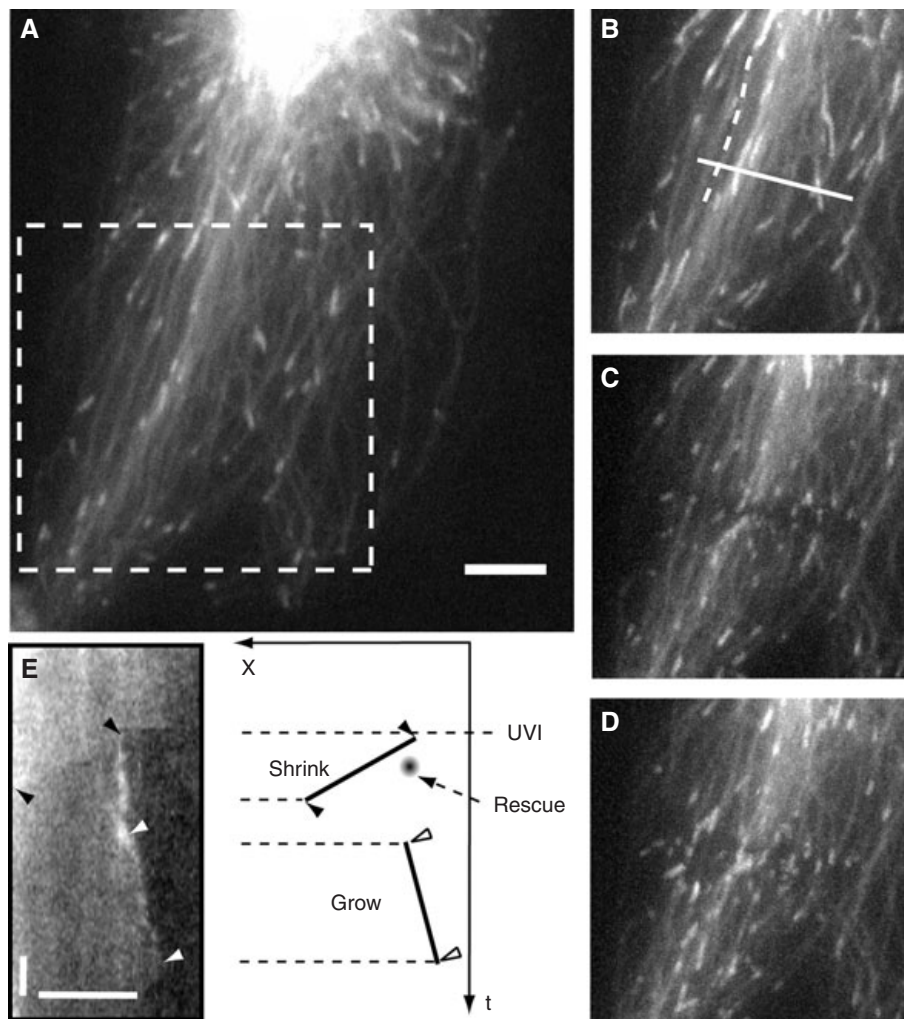


Figure 3: Microtubule (MT) rescue and regrowth after laser-induced shrinkage. A) Fluorescence micrograph of a Ptk-2 cell stably transfected with yellow fluorescent protein (YFP)- α -tubulin and transiently transfected with GFP-EB3. The dashed square indicates the enlarged area shown in (B–D). B–D) Sequences of MT rescue and growth. The laser 12 μ m long target path is indicated (full white line) and was performed by 47 pulses at 200 nJ. B) Maximum intensity projection during 11 seconds prior to ultraviolet irradiation (UVI) (B) directly following the UVI (C) and during 16 seconds after UVI (D). E) Kymograph plotting the intensity along the MT axis (dashed line) versus time. Black arrowheads show the linear shrinkage of the YFP MT body, and white arrowheads indicate the MT-tip regrowth after UVI. On the right, a scheme shows the line tracks used to measure the growth and shrinkage rates along the spatial (x) and temporal (t) axes. See also Supplementary Video 3 available as part of the online article from http://www.traffic.dk/suppmat/6_11.asp. Scale bars: 5 μ m (horizontal) and 5 seconds (vertical in E).

now. We used TIRF (31) to estimate shrinkage and growth in unperturbed cells. Other works reported a partial description of dynamic instability by using MT tips GFP labels (32) or fluorescence recovery after photobleaching (FRAP) to remove the fluorescent background in the cell center (33) and to allow single MT tracking. However, those techniques allow only the measurement of at most two parameters at a time, excluding rescue and catastrophe frequencies, and are not selective in time and space.

Pulsed UV laser nanosurgery is a new method for the measurement of selected MT dynamic instability parameters *in vivo*. After severing MTs, we were able to analyze their shrinkage, growth and rescue rates with high resolution and specificity in time and space, providing the basis for a rigorous quantification analysis, which is in contrast to the classical imaging techniques that are limited by the few number of natural events, occurring randomly in the cell volume and during the cell cycle.

We measured the shrinkage rate throughout the entire cytoplasm extent (Figure 2E) of interphase Ptk-2 cells with three different labeling methods and observe 25%

faster shrinkage of Alexa-488-labeled tubulin as compared with rhodamine and YFP, which shrink at the same rate. This is the first direct measurement of Alexa-488-labeled MT shrinkage rate. While our results with rhodamine and YFP tubulins correlate with previous measurements (29) (Table 1) with identical rates, the hydrophilic nature of Alexa-488 seems to have an effect on MT dynamics, which has not been investigated yet. The large number of shrinkage events measured in this study allowed us to observe that in the case of microinjection the standard deviations show a 40% higher variability than in stably transfected cells which is, we believe, a consequence of the microinjection technique and suggests that stable transfection is a more appropriate labeling method, because it is less perturbing for the MTs dynamics. To further judge the accuracy of the technique in retrieving physiological standard deviations, one can compare the accuracy of a shrinkage rate measurement, i.e. the error on the kymograph linear fitting of about 5% (see Results), and the resulting standard deviations of shrinkage rates, which vary from 18 to 26%. The variability of shrinkage rates inside a single cell, where measurements could be performed in up to 10 different sites throughout the

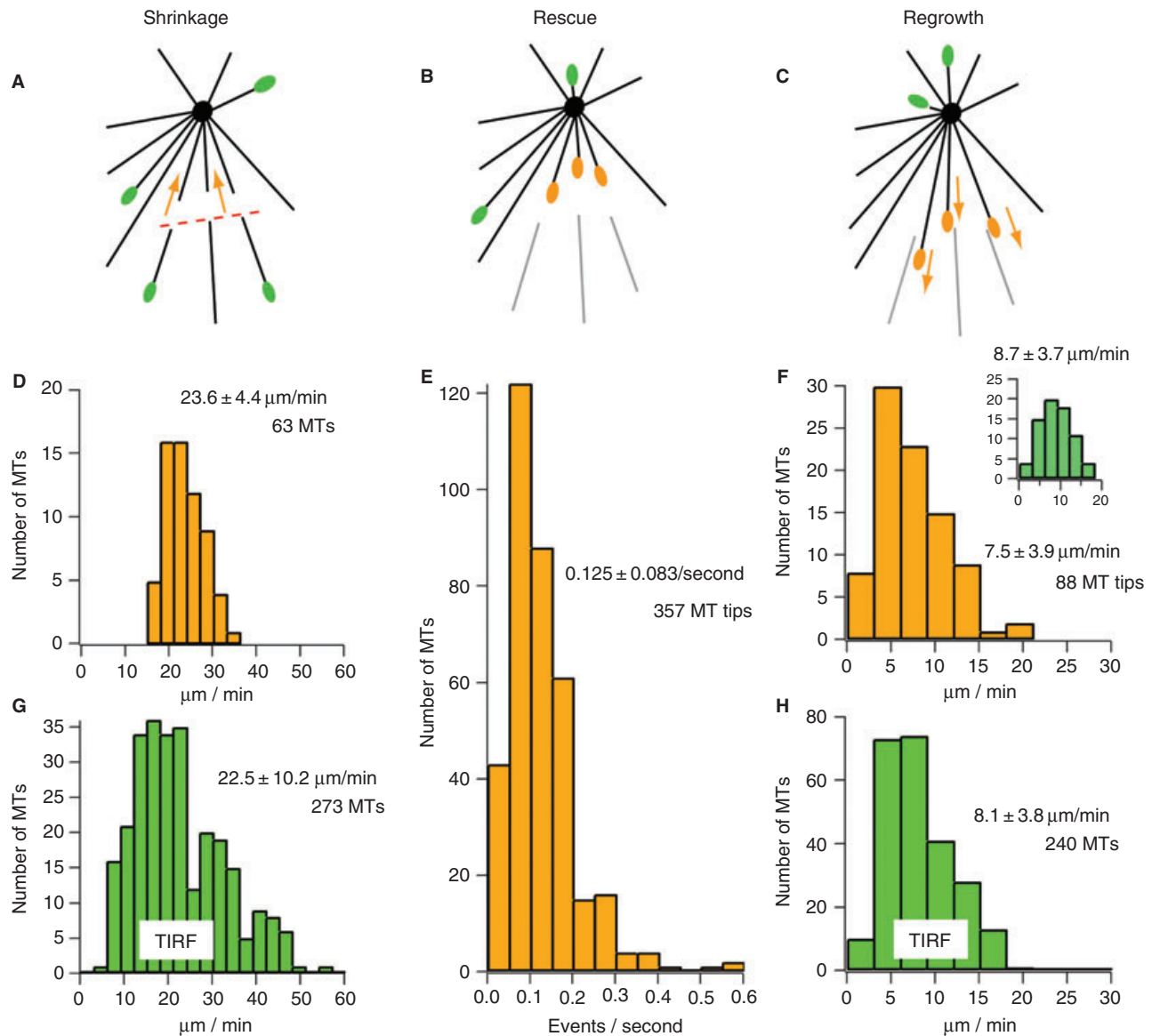


Figure 4: Three parameters of dynamic instability can be measured *in vivo*. A–C) Schematic sequence describing the measurement of shrinkage, rescue and regrowth after laser ultraviolet irradiation (UVI) from Figure 3. Green dots indicate the unaffected growing GFP-EB3 tips and orange dots the positions of the new tips growing after rescue. Orange arrows show the direction of microtubules (MTs) shrinkage and regrowth. D) Histogram of the yellow fluorescent protein (YFP)-tubulin MT shrinkage rate on the epi-fluorescence laser nanosurgery set up. E) Rescue frequency F_R distribution measured with all new tips appearance after UVI. F_R is calculated by taking the inverse of the time from the UVI to the tip appearing for each MT tip, i.e. from the artificial catastrophe to the rescue event. F) Growth rate of new GFP-EB3 tips. Histogram in the inset shows the distribution of the growth rate for unaffected MT tips outside the laser UVI area for comparison. G) Histogram of the YFP-tubulin MT shrinkage rate by total internal reflection fluorescence (TIRF) in unaffected cells. H) Histogram of the YFP-tubulin MT polymerization by TIRF in unaffected cells.

cytoplasm, is comparable with the variability between cells. This demonstrates that the values in Table 1 for Ptk-2 cells are representative for the phenomenon of shrinkage at any time point of the interphase stage and in any location throughout the cytoplasm.

Using a specific tip marker (GFP-EB3), we have been able to measure not only shrinkage but also, and simultaneously, two other parameters of dynamic instability, i.e.

growth rate and rescue frequency (Table 1). Growth rates of growing MT tips after UVI dissection are consistent with unperturbed growing EB3 tips with an about 17% slower growth after UVI and similar standard deviations. In contrast to the classical approach of rescue frequency measurement *in vitro* (7) or *in vivo* (28), which consists of averaging rescue events along the same MT in time, our approach consisted of following a single MT tip rescue event for a high number of MTs ($n = 357$) after an induced

Table 1: Comparison of dynamic instability parameters in interphase culture cells studied by laser nanosurgery and conventional imaging techniques

Dynamic instability parameter	Interphase mammalian LLCPK-1 cells [Rusan et al. (29)]		Interphase newt lung cells [Cassimeris et al. (28)]		Interphase mammalian Ptk-2 cells (this study)			Epi-fluorescence	
	Live imaging	EGFP tubulin	DIC live imaging	YFP tubulin stably transfected	Rhodamine tubulin microinjected	Alexa 488 tubulin microinjected	EB3 GFP transfected	EB3 GFP transfected	TIRF imaging
Number of cells	NP	NP	NP	34	36	40	40	32	29
ShrinkageRate ($\mu\text{m}/\text{min}$)	14.8 ± 8.54 (42)	13.1 ± 8.43 (62)	17.3 ± 0.7 (35)	19.5 ± 3.9 (106)	20.9 ± 5.5 (136)	25.4 ± 5.4 (131)	23.6 ± 4.4 (63)	-	22.5 ± 10.2 (273)
Growth Rate ($\mu\text{m}/\text{min}$)	11.50 ± 7.14 (42)	11.50 ± 7.40 (62)	7.2 ± 0.3 (42)	-	-	-	7.5 ± 3.9 (88)	8.7 ± 3.7 (72)	8.1 ± 3.8 (240)
RescueFrequency (per second)	0.203 ± 0.092	0.175 ± 0.104	0.044	-	-	-	0.125 ± 0.083 (357)	-	-
CatastropheFrequency (per second)	0.035 ± 0.024	0.026 ± 0.024	0.014	-	-	-	-	-	-

TIRF, total internal reflection fluorescence; YFP, yellow fluorescent protein; DIC, Differential Interference Contrast; NP, Not Provided.

catastrophe event. Both procedures should be statistically equivalent, provided that the number of measurements is high, and the values retrieved in this study are similar to results from previous study in mammalian interphase cells (Table 1).

To confirm that the parameters of dynamic instability retrieved by laser nanosurgery do correspond to physiological values and do not reflect an artifact introduced by the UVI procedure, we performed growth and shrinkage analyses by the use of TIRF with Ptk-2 cells stably transfected with YFP tubulin. Compared with the growth rate of GFP-EB3-labeled tips after UVI, the polymerization rate of unperturbed MTs as measured by TIRF is slightly lower, with a difference of only about 6% in mean value and with comparable variances. The shrinkage rate of non-irradiated YFP MTs is 15% higher than their laser-induced counterparts (see Discussion below). Both of these values are in good agreement with values measured in interphase newt lung cells (28) (Table 1). The measurement of catastrophe frequency was not performed in this study, even though it is technically possible to follow a full cycle of dynamic instability from the laser-induced catastrophe through the phases of shrinkage, rescue and growth up to the next catastrophe. Reasons for this are given by experimental evidences (33) showing a persistent growth phase of nascent MTs from the centrosome to the cell margin without catastrophe event, suggesting that a catastrophe measurement following rescue after laser UVI would be biased by the position of the cut.

In the context of the dynamic instability model (7,8), our results can be closely related to the GTP-cap model and the MT rescue. In our experiments, it is reasonable to assume that artificial catastrophes were induced relatively far away from the MT tips. As shown in Figure 3, the number of rescued MTs after UVI is much higher than the number of present growing tips prior to UVI. We therefore induced catastrophes mainly in a GDP tubulin lattice. Such a break in the MT lattice leads to a depolymerization of the MT plus end due to the unstable 'curved' conformation of GDP tubulin dimers, and to a more stable minus end. The GTP-cap model introduced by dynamic instability (7,8) can explain the shrinkage phenomenon after induced catastrophe due to a GDP protofilament curling up. However, it is somehow harder to interpret the observed rescue events of our experiments, performed away from the tip, i.e. away from a GTP cap. A recent theoretical study (34) proposed a purely structural model for MT capping and interpreted rescue events as a result of random thermal fluctuations relaxing the GDP MT lattice. Our measurements of rescue events performed in the middle of the GDP MT lattice could be an experimental evidence of the random nature of MT rescue. Their theoretical model also discusses structural reasons for the existence of a 'third state' in which MTs are neither growing nor shrinking, but rather rest in pause phase. In Figure 3(E), this phenomenon was actually observed.

Rescue occurs before regrowth starts, and both phenomena can be delayed. The experimental procedure consisting of inducing artificial catastrophes on MTs therefore provides quantitative evidences that seem to support modern theories of structural MT dynamics.

Another important aspect of our results is that the dynamic instability model does not explain the discrepancy between the laser-induced shrinkage measurements and their TIRF counterparts. By carefully comparing the shrinkage rate after UVI (Figure 2C) and the one observed in the TIRF experiments (Figure 4G) using the same YFP tubulin fusion cells, one can observe a striking difference. Both measurements give rise to a main peak at about 20 $\mu\text{m}/\text{min}$, while unperturbed cells show additional and up to twice as fast shrinkage rates. We estimate that in the unperturbed experiment, about 25% of the measured shrinkage events were faster than the average, i.e. generating side peaks above 30 $\mu\text{m}/\text{min}$ in Figure 4(G). The laser-induced measurements were performed all throughout the axial extent of the cell and do not show this behavior. We observe, therefore, that the unperturbed measurements performed with TIRF through a 100 nm axial extent from the glass substrate point at a faster shrinkage for a subset of MTs located at, or assembling close to, the plasma membrane. We propose two interpretations for this. First, such a discrepancy could be artificially induced by the limited depth of field which does not allow one to fully discriminate between MT shrinkage and the effect of a MT moving out of the plane of detection. Second, a subset of MTs could show different depolymerization dynamics in the membrane vicinity. It is reasonable to say that such different behavior would be hardly visible in the laser nanosurgery experiments, as they are performed in widefield through a cytoplasmic axial extent of about 1–3 μm , therefore, in a volume at least one order of magnitude larger. We are in favor of the second interpretation suggesting that MT assembly and dynamics could be influenced by the vicinity of the plasma membrane, as discussed in a recent review (35).

It has been reported earlier that MTs can be dissected in eukaryote cells by pulsed UV-B (36) and visible (17) laser radiation and undergo regrowth after irradiation (36), but a statistically relevant quantification of the reaction of MTs to UV laser irradiation was never achieved. Moreover, previous applications of intracellular laser surgery have assessed cellular viability only over a short time scale. In contrast, we were able to measure the parameters of MT dynamics with unprecedented accuracy, while the viability of the cells is not altered even 24 h after UVI. This demonstration addresses traditional concerns shared by many cell biologists that laser UV intracellular surgery could induce non-specific damage control mechanism such as activation of the p53 pathway (37).

We have introduced UVI nanosurgery as a robust and non-invasive technique that provides rigorous protocols to

study the interphase cytoskeleton from a quantitative point of view, in contrast to the classical qualitative MTs studies. Moreover, our instrument (23) is cost effective, in contrast to ultrashort pulsed lasers systems used recently in intracellular surgery (17,18,20–22) which represent a major financial investment for a research group, while a pulsed UV laser comes at a price that is five to 10 times lower.

Our study demonstrates that pulsed UV laser nanosurgery can be applied to the local investigation of intracellular dynamic polymers. Being able to investigate biopolymers in a spatiotemporally confined manner provides means for the analysis of the entire cytoskeleton during specific phases of cellular events such as migration and division. In particular, the confined measurement of the dynamic instability parameters will be an important feature when studying the regulation of specific MT-interacting proteins (MAPs) and their stabilizing or destabilizing functions during the interphase.

Materials and Methods

Optical set-up and laser nanosurgery

Microtubule and actin severing by plasma-induced ablation can be achieved with a frequency tripled Nd:YAG-pulsed laser (JDSUniphase, Grenoble, France), at a wavelength of 355 nm and a theoretical pulse duration of less than 500 ps. The beam was coupled through the epifluorescence port of a conventional Zeiss inverted microscope (Carl Zeiss, Göttingen, Germany) to allow simultaneous UVI and imaging and was focused with a high numerical aperture objective lens, a Zeiss C-Apochromat 63x/1.2 Water immersion. The efficient volume inside which laser damage occurred was estimated in glass to be about 5.2 times the extent of the focal volume (23) with a lateral extent of about to 450 nm. All irradiations were performed along a manually defined spline-line laser target, defined interactively on the image with a graphical mouse interface, along which laser pulses were distributed. Pulse density along the line was set such that the optical intensity is approximately constant. This was achieved by placing the maxima of two neighboring pulses at a distance equal to the diffraction limit beam half-width. Consequently, the spatial pulse pitch was 180 nm, and the distribution is described by a linear density of 5.5 pulses per μm at a speed of 100–1000 pulses per second. In this study, MT and actin severing was successful with single spline irradiation with energy in the range of 50–200 nJ per pulse, corresponding to a central peak power density ranging from 133 to 530 GW/cm².

Measurements and live imaging

Simultaneous irradiation and live imaging of cells was performed on a Zeiss Axiovert 200M microscope with a Hamamatsu ORCA CCD camera (Hamamatsu Photonics KK, Hamamatsu City, Japan), which allowed low-light-level fluorescence imaging with a frame rate up to four frames per second. Microtubule polymerization dynamics with nanosurgery and TIRF experiments were measured with kymographs (<http://www.embl.de/eamnet/>) by plotting the intensity distribution along the MT axis versus time. Constant velocities appeared as a linear contrast difference, which can then be fitted by a line whose slope gives the rate of polymerization or depolymerization.

TIRF imaging, i.e. the selective illumination of a thin sheet of the cell close to the lower surface (31), was performed on an Olympus Biosystems Cell-R-automated microscope set-up (Olympus Biosystems, Munich, Germany) equipped with a 488 nm Coherent Sapphire Diode laser (Coherent, Santa Clara, CA, USA), using an Olympus 1.45 NA PlanApo 'TIRF' Objective lens. The depth of field was about 100 nm.

Cell temperature was controlled using a Zeiss heating stage insert set at 37 °C. Epifluorescence and laser UVI experiments were performed using cells in imaging medium (DMEM, 10% fetal calf serum, 25 mM Hepes pH 7.4, 2 mM L-Glutamine) and imaged for not more than 45 min for each sample, whereas TIRF experiments were performed without changing the incubation medium (Red Phenol).

Cell lines, microinjection and transfection

Wild-type Ptk2 cells were grown in DMEM supplemented with 10% fetal bovine serum under standard tissue culture conditions. All cell-culture media and sera were obtained from Invitrogen (Carlsbad, CA, USA). Ptk2 cells stably expressing tagged tubulin-YFP were maintained in the presence of 0.45 mg/mL G-418 sulfate. Cells were plated onto glass bottom dishes (MatTek, Ashland, MA, USA). Purified Alexa-488 tubulin or rhodamine tubulin were prepared in HKCl microinjection buffer (10 mM HEPES, 140 mM KCl, pH 7.4) and microinjected into the cytoplasm at 5 $\mu\text{g}/\text{mL}$ with back-loaded glass capillaries using an Eppendorf micromanipulator and transjector, typically followed by 1 h recovery time in an incubator. During microinjection, cells were maintained at room temperature in CO₂-independent medium (MEM without phenol red but containing 30 mM Hepes, Gibco-BRL, Karlsruhe, Germany), and between 100 and 200 cells were injected per cover slip.

Actin-GFP and EB3-GFP expression constructs (0.6 μg each) were transfected using 2.6 μL of FuGene 6 Transfection Reagent (Roche, Indianapolis, IN, USA) per dish. In all our experiments, only low expressing cells were considered for dynamical study.

Acknowledgments

The authors thank Mirco Castoldi for providing Rhodamin tubulin, Matthias Utz for Alexa-488 tubulin, Niels Galjart for the kind gift of EB3-GFP, Alfons Riedinger for the software development, Carl Zeiss (Germany) for providing the microscope apparatus and Olympus BioSciences GmbH and Dr Andreas Pfuhl (Olympus Europe) for permanent support of the ALMF. We thank Thomas Surrey, Eric Karsenti and Jim Swoger for critical comments. This research was partially supported by the VDI-TZ and the German ministry for research and development (BMBF) by grant FKZ 13N8287.

References

1. Alberts A, Johnson A, Lewis J, Raff M, Roberts K, Walter P. Molecular Biology of the Cell, 4th edn. New York: Garland Science; 2002.
2. Wesselman JPM, De Mey JGR. Angiotensin and cytoskeletal proteins: role in vascular remodeling. *Curr Hypertens Rep* 2002;4:63–70.
3. Brandt R. Cytoskeletal mechanisms of neuronal degeneration. *Cell Tissue Res* 2001;305:255–265.
4. Garcia ML, Cleveland DV. Going new places using an old map: tau, microtubules and human neurodegenerative disease. *Curr Opin Cell Biol* 2001;13:41–48.
5. Condeelis JS, Wyckoff JB, Bailly M, Pestell R, Lawrence D, Backer J, Segall JE. Lamellipodia in invasion. *Semin Cancer Biol* 2001;11:119–128.
6. Thiery JP, Chopin D. Epithelial cell plasticity in development and tumor progression. *Cancer Metastasis Rev* 1999;18:31–42.
7. Mitchison TJ, Kirschner M. Dynamic instability of microtubule growth. *Nature* 1984;312:237–242.
8. Desai A, Mitchison TJ. Microtubule polymerization dynamics. *Annu Rev Cell Dev Biol* 1997;13:83–117.
9. Kinoshita K, Arnal I, Desai A, Drechsel DN, Hyman AA. Reconstitution of physiological microtubule dynamics using purified components. *Science* 2001;294:1340–1343.

10. Wilson L, Panda D, Jordan MA. Modulation of microtubule dynamics by drugs: a paradigm for the actions of cellular regulators. *Cell Struct Funct* 1999;24:329–335.
11. Grill SW, Howard J, Schäffer E, Stelzer EHK, Hyman AA. The distribution of active force generators controls mitotic spindle position. *Science* 2003;301:518–521.
12. Grill SW, Gönczy P, Stelzer EHK, Hyman AA. Polarity controls forces governing asymmetric spindle positioning in the *Caenorhabditis elegans* embryo. *Nature* 2001;409:630–633.
13. Aist JR, Liang H, Berns MW. Astral and spindle forces in PtK2 cells during anaphase B: a laser microbeam study. *J Cell Sci* 1993;104:1207–1216.
14. Spurck TP, Stonington OG, Snyder JA, Pickett-Heaps JD, Bajer A, Mole-Bajer J. UV microbeam irradiations of the mitotic spindle. II. Spindle fiber dynamics and force production. *J Cell Biol* 1990;111:1505–1518.
15. Chen W, Zhang D. Kinetochores fibre dynamics outside the context of the spindle during anaphase. *Nat Cell Biol* 2004;6:227–231.
16. Maiato H, Khodjakov A, Rieder CL. *Drosophila* CLASP is required for the incorporation of microtubule subunits into fluxing kinetochores fibres. *Nat Cell Biol* 2004;7:42–47.
17. Botvinick EL, Venugopalan V, Shah JV, Liaw LH, Berns MW. Controlled ablation of microtubules using a picosecond laser. *Biophys J* 2004;87:4203–4212.
18. Tolić-Nørrelykke IM, Sacconi L, Thon G, Pavone FS. Positioning and elongation of the fission yeast spindle by microtubule-based pushing. *Curr Biol* 2004;14:1181–1186.
19. Khodjakov A, La Terra S, Chang F. Laser microsurgery in fission yeast: role of the mitotic spindle midzone in anaphase B. *Curr Biol* 2004;14:1330–1340.
20. Watanabe W, Arakawa N, Matsunaga S, Higashi T, Fukui K, Isobe K, Itoh K. Femtosecond laser disruption of subcellular organelles in a living cell. *Opt Express* 2004;12:4203–4213.
21. König K, Riemann I, Fritzsche W. Nanodissection of human chromosomes with near-infrared femtosecond laser pulses. *Opt Lett* 2001;26:819–821.
22. Yanik MF, Cinar H, Cinar HN, Chisholm AD, Jin YS, Ben-Yakar A. Neurosurgery – functional regeneration after laser axotomy. *Nature* 2004;432:822.
23. Colombelli J, Grill SW, Stelzer EHK. Ultraviolet diffraction limited nano-surgery of live biological tissues. *Rev Sci Instr* 2004;75:472–478.
24. Vogel A, Venugopalan V. Mechanisms of pulsed laser ablation of biological tissues. *Chem Rev* 2003;103:577–644.
25. Nakagawa H, Koyama K, Murata Y, Morito M, Akiyama T, Nakamura Y. EB3, a novel member of the EB1 family preferentially expressed in the central nervous system, binds to a CNS-specific APC homologue. *Oncogene* 2000;19:210–216.
26. Pepperkok R, Bre MH, Davoust J, Kreis TE. Microtubules are stabilized in confluent epithelial cells but not in fibroblasts. *J Cell Biol* 1990;111:3003–3012.
27. Khodjakov A, Rieder CL, Mannella CA, Kinnally KW. Laser micro-irradiation of mitochondria: is there an amplified mitochondrial death signal in neural cells? *Mitochondrion* 2004;3:217–227.
28. Cassimeris L, Pryer NK, Salmon ED. Real-time observations of microtubule dynamic instability in living cells. *J Cell Biol* 1988;107: 2223–2231.
29. Rusan NM, Fagerstrom CJ, Yvon AM, Wadsworth P. Cell cycle-dependent changes in microtubule dynamics in living cells expressing green fluorescent protein- α tubulin. *Mol Biol Cell* 2001;4: 971–980.
30. Waterman-Storer CM, Desai A, Bulinski JC, Salmon ED. Fluorescent speckle microscopy, a method to visualize the dynamics of protein assemblies in living cells. *Curr Biol* 1998;8:1227–1230.
31. Steyer JA, Almers W. A real-time view of the life within 100 nm of the plasma membrane. *Nat Rev Mol Cell Biol* 2001;2:268–275.
32. Piehl M, Cassimeris L. Organization and dynamics of growing microtubule plus ends during early mitosis. *Mol Biol Cell* 2003;14:916–925.
33. Komarova YA, Vorobjev IA, Borisy GG. Life cycle of MTs: persistent growth in the cell interior, asymmetric transition frequencies and effects of the cell boundary. *J Cell Sci* 2002;115:3527–3539.
34. Janosi IM, Chrétien D, Flyvbjerg H. Structural microtubule cap: stability, catastrophe, rescue and the third state. *Biophys J* 2002;83: 1317–1330.
35. Small JV, Geiger B, Kaverina I, Bershadsky A. How do microtubules guide migrating cells? *Nat Rev Mol Cell Biol* 2002;3:957–964.
36. Tao W, Walter RJ, Berns MW. Laser-transected microtubules exhibit individuality of regrowth, however most free new ends of the microtubules are stable. *J Cell Biol* 1988;107:1025–1035.
37. Harris SL, Levine AJ. The p53 pathway: positive and negative feedback loops. *Oncogene* 2005;24:2899–2908.